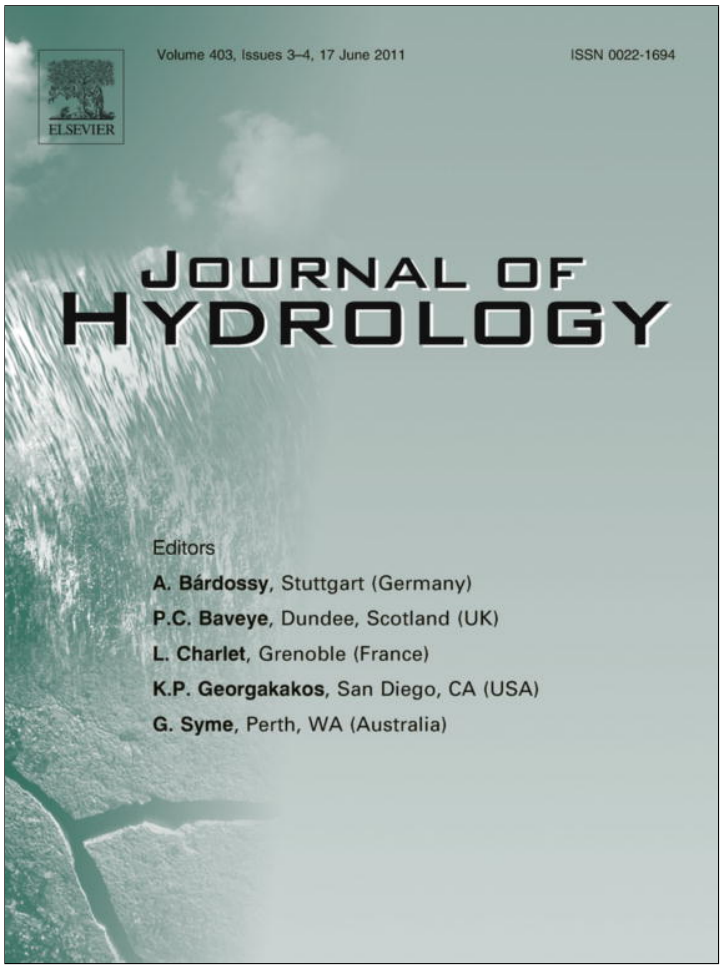

Journal of Hydrology 403 (2011) 242–252

Contents lists available at ScienceDirect

Journal of Hydrology

journal homepage: www.elsevier.com/locate/jhydrol

Localization and quantification of leakages in dams using time-lapse self-potential measurements associated with salt tracer injection

A. Bolève [a,b,*], F. Janod [a], A. Revil [b,c], A. Lafon [a], J.-J. Fry [d]

[a] FUGRO, Savoie Technolac, Le Bourget-du-Lac Cedex, France
[b] ISTerre, CNRS (UMR 5559), Université de Savoie, Equipe Volcan, Le Bourget-du-Lac, France
[c] Colorado School of Mines, Dept. of Geophysics, Golden, CO, USA
[d] EDF-CIH, Savoie Technolac, Le Bourget-du-Lac, France

ARTICLE INFO

Article history:
Received 12 June 2010
Received in revised form 13 February 2011
Accepted 3 April 2011
Available online 12 April 2011
This manuscript was handled by P. Baveye, Editor-in-Chief

Keywords:
Self-potential
Brine
Streaming potential
Leakage
Dams
Monitoring

SUMMARY

The self-potential method is the only non-intrusive method that is directly sensitive to the flow of the pore water in a porous material. We propose the use of a new protocol of self-potential measurements associated with a brine injection to locate leakages in earth dams and to quantify their permeability. Indeed, a brine solution injection upstream of an earth dam (in the assumed leakage zone) is able to change the electrical conductivity of the medium. In turn, this decreases the magnitude of the electrokinetic contribution of the self-potential signals that are related to the flow of the seepage water. The evolution of this anomalous self-potential signal (expected to be positive with respect to a reference state prior the salt injection) can be measured at the ground surface with a network of non-polarizing electrodes. The seepage flow inside the dam is localized from the evolution in space and time of the resulting transient self-potential signals associated with the transport of the brine. The mean permeability of the preferential flowpath can be determined. This method is first applied to a laboratory test to show how the passage of a salt tracer affects the self-potential response. Then, we apply this new methodology to a field test site (a dam with a proven leakage) located in the south of France. At this test site, self-potential mapping was first performed to locate the preferential flow path. Then, a network of non-polarizing electrodes was used to perform time-lapse self-potential measurements at the dam crest during a brine injection occurring upstream of the seepage zone. We used two lines of 16 non-polarizing electrodes each. From the time-lapse data, the permeability of the leaking area was estimated inside one order of magnitude.

1. Introduction

Monitoring the stability of water retention structures like embankments and levees is an important issue regarding the security of populations living in their vicinities (Fell et al., 1992; Wan and Fell, 2008). This implies the necessity to characterize preferential pathways associated with internal erosion that can mechanically weaken these structures. Geophysical studies have been applied to map and image preferential fluid flow pathways in embankments and levees or in their foundations (e.g., Gex, 1980; Panthulu et al., 2001; AlSaigh et al., 1994; Rozycki et al., 2006; Rozycki, 2009; Sheffer, 2007; Bolève et al., 2009; Sheffer, 2002). Time-lapse electrical resistivity tomography (ERT) is a non-intrusive method able to identify preferential flow paths associated with internal erosion mechanisms (Titov et al., 2000; Sjodahl et al., 2005, 2006). ERT has also been applied successfully to tracer tests to characterize heterogeneous aquifers (Müller et al., 2010). So, it is tempting to use time-lapse ERT to monitor a salt tracer injection through a leaking embankment to characterize the permeability along the flow paths. However, taking a snapshot with electrical resistivity tomography can be time-prohibitive, especially for leakages characterized by high flow rates. In order to identify leakage signatures in water retention structures, we need to use some passive methods that are directly sensitive to the seepage as well as the presence of salt in the pore water. The self-potential method (Nourbehecht, 1963; Sill, 1983; Corwin, 1985, 1997; Wilt and Corwin, 1989; Wurmstich et al., 1991) and temperature measurements (Rath and Mottaghy, 2007) are both sensitive to flow in porous media (see Jardani and Revil, 2009, for a joint inversion of these two types of data to recover the flow field). Self-potential is a non-intrusive method and because the electromagnetic diffusivity is much smaller than the thermal diffusivity it can be used to follow in real-time the transport of salt through a porous material (Revil and Jardani, 2010). In addition, the physics of the self-potential signals associated with the transport of a salt tracer is well-established (Revil and Jardani, 2010; Martínez-Pagán et al., 2010).

* Corresponding author at: FUGRO, Savoie Technolac, Le Bourget-du-Lac Cedex, France.
E-mail address: alexandre.boleve@gmail.com (A. Bolève).

0022-1694/$ - see front matter © 2011 Elsevier B.V. All rights reserved.
doi:10.1016/j.jhydrol.2011.04.008

The occurrence of self-potential signals with the flow of the ground water can be understood as follows. The surface of mineral grains in contact with water is generally negatively charged (e.g., Kosmulski and Dahlsten, 2006). In order to compensate for the imbalance of electrical charges attached to the mineral grains, an excess of electrical charges exists in the vicinity of the mineral surface in the so-called electrical double layer (Helmholz, 1879; Nourbehecht, 1963; Revil and Leroy, 2004). The mobile part of this excess of electrical charges (located in the so-called diffuse layer) is dragged by the flow of the pore water. The net flow of charges per unit surface area of a cross-section of a porous material and per unit time is an electrical current density proportional to the Darcy velocity. This source current density (called the streaming current) corresponds to a source term in the Maxwell equations for both an electrical field and a magnetic field. The electrical field can be measured at the ground surface with a set of non-polarizing electrodes and a high input impedance voltmeter (typically 100 MΩ and a sensitivity of 0.1 mV). The distribution of the equipotentials created by the source current density is also shaped by the distribution of the electrical resistivity. The polarity, as well as the magnitude of the electrical field (called the streaming potential), can give indications on the direction and the velocity of the leakage flow (e.g., Nourbehecht, 1963; Bogoslovsky and Ogilvy, 1970; Bolève et al., 2009; and Revil and Jardani, 2010).

The methodology presented in the present paper follows therefore the previous ideas to answer the following question: Why not use time-lapse self-potential measurements to monitor a salt tracer injection at an embankment in real time? Such an approach could be used not only to locate in real time areas of preferential fluid flow pathways (overcoming the limitations of DC resistivity tomography) but also to estimate the permeability, seepage velocity and geometrical evolution of the flow path over time. This new methodology (self-potential monitoring associated with brine injection upstream) is developed below and tested both in the laboratory and in the field.

2. Theoretical background

The classical formulation of the coupled hydro-electrical flow in a porous media (including streaming current and electroosmosis) is based on a linear formulation of two coupled constitutive equations for the electrical current density and the seepage velocity (Darcy velocity) obeying Onsager's reciprocity to satisfy positive dissipation. This approach is traditional based on non-equilibrium thermodynamics (Mitchell, 1993; Revil, 2007) but can be also based on upscaling methods like the volume-averaging approach (Revil and Linde, 2006). The streaming current density is related to the gradient of the pore fluid pressure through a streaming current coupling coefficient that depends on the so-called zeta potential. The zeta potential is an electro-chemical parameter of the electrical double layer coating the surface of minerals in contact with pore water (e.g., Ishido and Mizutani, 1981; Leroy and Revil, 2004). The flow of the pore water and the current density are two fluxes that are coupled together through the following constitutive equations (Ishido and Mizutani, 1981; Morgan et al., 1989; Revil et al., 1999a,b)

$$\mathbf{j} = -\sigma\nabla\varphi - L\nabla(p - \rho_f\mathbf{g}), \tag{1}$$

$$\mathbf{u} = -L\nabla\varphi - \frac{k}{\eta_f}\nabla(p - \rho_f\mathbf{g}) \tag{2}$$

$$C = \left(\frac{\partial\varphi}{\partial p}\right)_{j=0} = -\frac{L}{\sigma} \approx \frac{\varepsilon_f\zeta}{\eta_f\sigma_f}, \tag{3}$$

where $\mathbf{j}$ is the total current density (A m^{-2}), $\mathbf{u}$ is the Darcy velocity (m s^{-1}), p is the pore fluid pressure (Pa), $\mathbf{g}$ is the gravity acceleration vector (m s^{-2}), ρ_f is the mass density of the pore water (kg m^{-3}) and η_f is the dynamic shear viscosity (Pa s). $E = -\nabla\varphi$ is the electrical field in the quasi-static limit of the Maxwell equations (V m^{-1}) (for which the electrical and magnetic fields are not coupled by induction) and φ the electrical potential (V). There are three material properties entering into Eqs. (1) and (2); the electrical conductivity σ (in S m^{-1}), the streaming current coupling coefficient L (m^2 V^{-1} s^{-1}), and the permeability k (m^2). The first part of Eq. (3) defines the streaming potential coupling coefficient C (V Pa^{-1}) and the last part corresponds to the Helmholtz–Smoluschowski equation for which ε_f is the dielectric constant of the pore water (in F m^{-1}) ζ is the so-called ζ-potential (in V, a key electrochemical property of the pore water mineral interface, e.g., Leroy and Revil, 2009), and η_f is the dynamic viscosity of water (in Pa s). The streaming current density is defined by $j_S = -L\nabla p$.

Neglecting the electroosmotic contribution in the Darcy equation (an excellent approximation in absence of external sources of current, Sill, 1983; Revil et al., 1999b), Eq. (1) can also be expressed in another way by the following equation, which takes directly into account the Darcy velocity $\mathbf{u}$ (Revil and Leroy, 2004, and Revil and Linde, 2006):

$$\mathbf{j} = \sigma\mathbf{E} + \overline{Q}_v\mathbf{u}, \tag{4}$$

where $\overline{Q}_v$ is the excess electrical charge (of the electrical diffuse layer) per unit pore volume located in the pore water (in C m^{-3}). In this case, Eq. (2) can thus be simplified as follows:

$$\mathbf{u} = -\frac{k}{\eta_f}\nabla(p - \rho_f\mathbf{g}) = -K\nabla(H + z). \tag{5}$$

In Eq. (5), K is the hydraulic conductivity (m s^{-1}), H is the pressure head (in m) and z the elevation (in m). The previous set of constitutive equations can be used to give the following expressions of the source current density and the streaming potential coupling coefficient (see Bolève et al., 2009):

$$\mathbf{j}_s = \sigma C\nabla p = -\frac{\sigma C\eta_f}{k}\mathbf{u}, \tag{6}$$

$$C = \frac{-Q_v k}{\sigma\eta_f}. \tag{7}$$

Eq. (7) provides an alternative to the Helmholtz–Smoluchowski equation given above (second part of Eq. (3)). The continuity equation for the electrical charges in the quasi-static limit of the Maxwell-equations is expressed as:

$$\nabla\cdot\mathbf{j} = 0. \tag{8}$$

Therefore, the electrical current density is conservative in the quasi-static limit of the Maxwell equations. By combining Eqs. (4) and (8), we obtain a Poisson equation for the electrical potential,

$$\nabla\cdot(\sigma\nabla\varphi) = \Im, \tag{9}$$

where the volumetric current density source, $\Im$, is given by:

$$\Im = \overline{Q}_v\nabla\cdot\mathbf{u} + \nabla\overline{Q}_v\cdot\mathbf{u}. \tag{10}$$

Eq. (10) shows two types of electrical sources as already discussed by Sill (1983). The first source of electrical signal is related to the divergence of the fluid flow. The second corresponds to areas or interfaces where there is a gradient (or a drop) of the excess electrical charge density per unit pore volume in the pore space. Under steady-state conditions and without sinks/sources of fluid flow, $\nabla\cdot\mathbf{u} = 0$ and the only source term corresponds to the second part of Eq. (10). This yield,

$$\Im = \nabla \overline{Q}_v \cdot \mathbf{u}. \tag{11}$$

The excess charge density $\overline{Q}_v$ can be obtained directly from the permeability by (Jardani et al., 2007; Bolève et al., 2009):

$$\log(\overline{Q}_v) = -9.2349 - 0.8219 \log(k), \tag{12}$$

This relationship exists because both the permeability and the excess charge density are related to the specific surface area of the porous material.

We have also to consider the evolution of the conductivity of the pore water due to the injection of the brine solution. Because the volumetric source current density $\Im$ is very sensitive to the distribution of electric conductivity (see Eq. (9)), we also have to take into account the effect of a brine solution injection through a transport equation. The evolution of the electrical conductivity of the water can be expressed using the semi-empirical relation derived by Sen and Goode (1992):

$$\sigma_f(C_f;T) = (d_1 + d_2 T + d_3 T^2) C_f - \frac{d_4 + d_5 T}{1 + d_6 C_f} (C_f)^{3/2}, \tag{13}$$

where $d_1 = 5.6$, $d_2 = 0.27$, $d_3 = -1.51 \times 10^{-4}$, $d_4 = 2.36$, $d_5 = 0.099$, $d_6 = 0.214$, σ_f is the electrical conductivity of water (in S m^{-1}), T is the temperature (in °C) and C_f is the salinity (in mol L^{-1}).

The flow of water in the porous sand is governed by Darcy's law, (Eq. (5)). Inserting Darcy's law in the continuity equation for the mass of the pore water, the pressure follows the classical linear diffusion equation in saturated conditions (e.g., Bear, 1972):

$$\rho_f S \frac{\partial p}{\partial t} + \nabla \cdot \left[-\rho_f \frac{k}{\eta_f} \nabla (p - \rho_f \mathbf{g}) \right] = 0, \tag{14}$$

where S is the specific storage coefficient (s^2 m^2 kg^{-1}) and t is the time (in s).

The partial differential equation describing the transport of the salt is the diffusion/dispersion transport equation is given by,

$$\phi \frac{\partial c}{\partial t} + \nabla \cdot \left[-\phi \overline{\overline{D}}_L \cdot \nabla c + \mathbf{u} c \right] = 0, \tag{15}$$

where c is the salt concentration (mol L^{-1}) and $\overline{\overline{D}}_L$ is the hydrodynamic dispersion tensor (m^2 s^{-1}). The principal diagonal components D_{Lii} and non-diagonal components (cross-terms) of this tensor are,

$$\phi D_{Lii} = \alpha_1 \frac{u_i^2}{|\mathbf{u}|} + \alpha_2 \frac{u_j^2}{|\mathbf{u}|} + \frac{D_m}{\tau}, \tag{16}$$

$$\phi D_{Lij} = \phi D_{Lji} = (\alpha_1 + \alpha_2) \frac{u_i u_j}{|\mathbf{u}|}, \quad i \neq j, \tag{17}$$

respectively, where α_1 and α_2 are the longitudinal and transversal dispersivities (in m), respectively, τ is the tortuosity factor which decrease impact of molecular diffusion for porous media relative to free water, here $\tau = F\phi = 1.6$ and D_m is the mutual diffusion coefficient of NaCl in water (1×10^{-9} m^2 s^{-1}).

3. Laboratory experiment

We discuss below a laboratory test of our approach. We monitored a brine injection using time-lapse self-potential measurements in a sample made of sand, with a measured permeability of $k = (9 \pm 2) \times 10^{-11}$ m^2, an estimated porosity $\phi = 0.40$, and an electrical formation factor $F = 4$ (determined with Archie's law $F = \phi^{-m}$ using a cementation exponent $m = 1.5$ valid for sand). If the surface conductivity associated with electrical conduction along the pore water/mineral interface can be neglected, the electrical conductivity of a porous material is given by (Revil et al., 1998),

$$\sigma = \sigma_f Du, \quad \text{as } Du \geqslant 1, \tag{18}$$

$$\sigma = \frac{\sigma_f}{F} \left[FDu + \frac{1}{2}(1 - Du)\left(1 - Du + \sqrt{(1 - Du)^2 + 4FDu}\right) \right], \quad \text{as } Du \leqslant 1, \tag{19}$$

where σ is the sample conductivity (S m^{-1}) and F the electrical formation factor (dimensionless) and Du is a dimensionless number called the Duhkin number which represents the ratio between the surface conductivity of the grains σ_s and the electric conductivity of the pore water σ_f:

$$Du \equiv \sigma_S / \sigma_f. \tag{20}$$

For a packing of spheres of diameter d_0, the surface conductivity σ_s can be expressed as (Revil and Linde, 2006)

$$\sigma_s = \frac{6\Sigma_s}{d_0}, \tag{21}$$

where Σ_s is the specific surface conductivity (S) and the numerical constant 6 corresponds to spherical grains. The mean grain size diameter of the sand is 4×10^{-4} m. Using a specific surface conductivity Σ_s equal to 4×10^{-9} S (see Bolève et al., 2007), we estimate

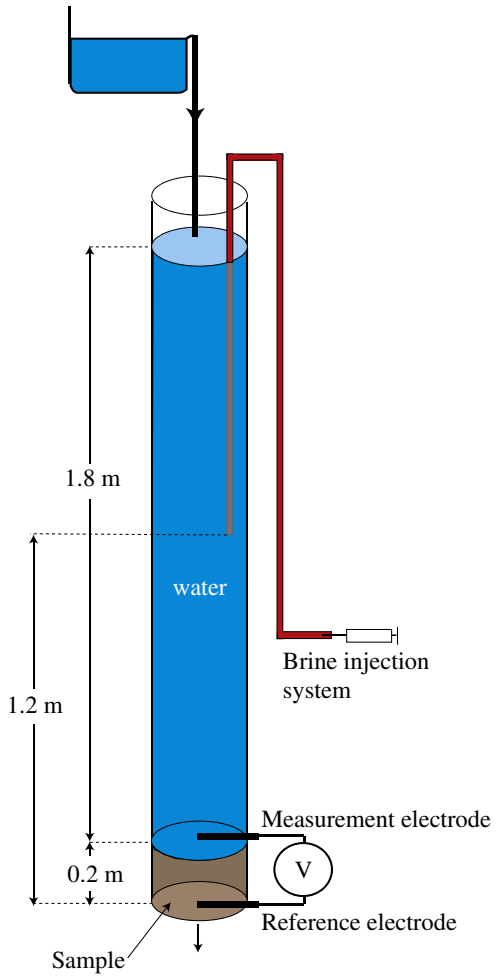

Fig. 1. Sketch of the laboratory brine injection experiment. A column experiment is used to investigate the change in the self-potential response during the passage of a brine. The sample, made of sand, is packed at the bottom of the Plexiglas column and is maintained in the column by a permeable membrane with a mesh finer than the diameter of the sand grains. The record of the self-potentials during the flow of the electrolyte through the sample is done with silver electrodes. The hydraulic heads are maintained constant during the two brine injections and the streaming potentials are recorded at the end-faces of the sample.

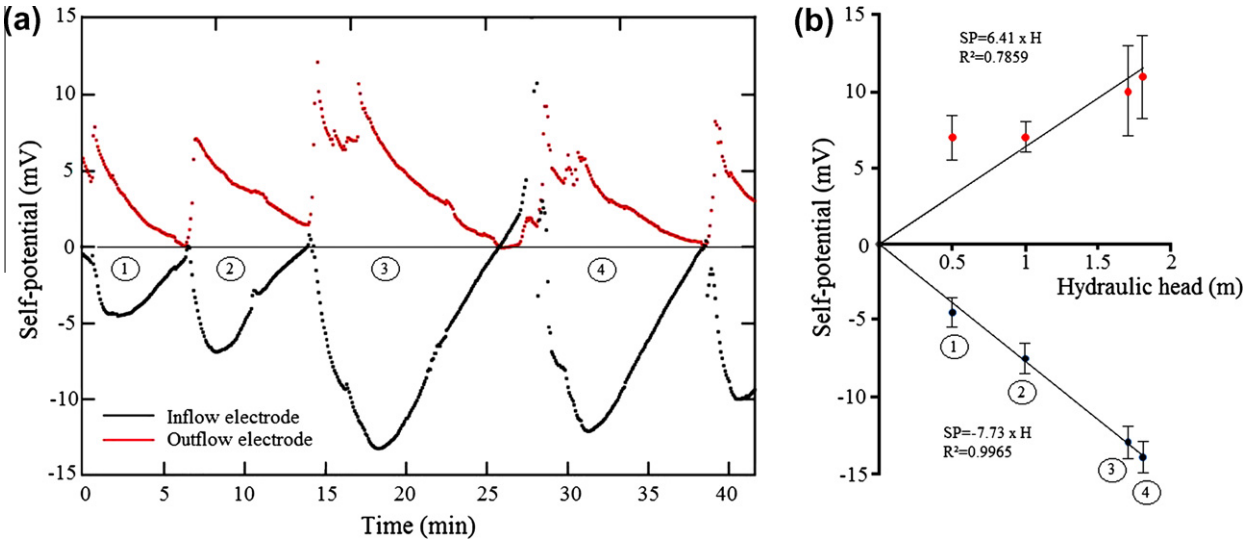

Fig. 2. (a) Experiment results corresponding to the four increases and decreases of the hydraulic head. Two silvers electrodes record the self-potential signal at both end-faces of the sand sample. The reference electrode is located at the mid-position inside the sample. Each cycle (cycle 1–4) corresponds to a maximum of head pressure inside the pipe of 0.5, 1, 1.8, and 1.7 m, respectively. We observe that the self-potential signal recorded by the outflow electrode is more perturbed than the signals recorded by the inflow electrode. (b) Self-potential signals versus the hydraulic heads. The linear relationship between the variation of the streaming potentials and the variation of the hydraulic heads provides the value of the streaming potential coupling coefficient C. Using the outflow electrode, we obtain $C_1 \approx -15.5$ mV m^{-1} and for the inflow electrode, we obtain $C_2 \approx -12.8$ mV m^{-1}.

the surface conductivity to 6×10^{-5} S m^{-1}. Consequently, the Dukhin number was estimated to be $Du \approx 2 \times 10^{-3}$ (indeed the expression under bracket in Eq. (19) is equal to 1.01). The influence of the Dukhin number becomes negligible for $Du < 1 \times 10^{-2}$ (see Crespy et al., 2007). Therefore neglecting surface conductivity is justified here and

$$\sigma \approx \frac{\sigma_f}{F}, \tag{22}$$

Note that the influence of the surface conductivity upon the streaming potential coupling coefficient can be important in presence of clay minerals. A high surface conductivity would decrease the streaming potential coupling coefficient and would therefore impact the self-potential signals recorded during an experiment.

For our experiment, we used a vertical column made of Plexiglas filled at its bottom by 20 cm of compacted saturated sand (Fig. 1). The sand sample was previously washed (using the same water which was used during all experiment) to remove any residual clays. Before to perform the brine injection experiment, we first tested the experiment protocol using four increases/decreases water level cycles without any salt solution injections. We used three silvers rods (length of 3 cm) to record the electrical potentials. The reference electrode was located in the middle of the sand sample (length of 20 cm) while two others electrodes (terminal electrodes) were located at the two end-faces of the cylindrical sample. Fig. 2 and Table 1 provides the experimental results in terms of water level and self-potential measurements for the two terminal electrodes. A linear relationship between water pressure level and the magnitude of the self-potential signals exists indicating that our protocol is reliable for the brine injection experiment. The excess of charges per unit pore volume $\overline{Q}_v$ can be also estimated from the measured electro-kinetic coupling coefficient and the measured electrical conductivity using Eq. (7). We obtained $\overline{Q}_v = 0.11 \pm 0.02$ C m^{-3} for the sand saturated with water (water conductivity of 0.025 S m^{-1} at 25 °C, $C = -15 \pm 1$ mV m^{-1}, see Fig. 2b).

The brine injection experiment can be described as follow. We first increased the water head inside the Plexiglas column until it reached 1.8 m. We maintained this hydraulic head constant during the duration of experiment. The self-potential signals were measured at the end faces of the core sample. The reference electrode was located at the downstream end-faces of the Plexiglas column. The electrical potential difference reached a constant value of −25 mV after 7 min. This negative signal is expected because the coupling coefficient is negative and positive charges are dragged along with the pore water flow. To study the transient effect of the brine solution (NaCl solution) upon the electrical potential signal the next step consisted of injecting two brine solutions at the center of the column. The first brine was injected at $t_1 = 9$ min after the beginning of the experiment and the second injection at $t_2 = 18$ min. The estimated volume of the brine injected is 5×10^{-5} m^3 with an electrical brine conductivity equal to 1.5 S m^{-1} at 25 °C. The self-potential signals were recorded using two silvers rods located through the Plexiglas pipe with a plastic membrane to avoid any leakage between the walls of the column and electrodes. We monitored the electrical self-potential variation with a data-logger (Easy Log, internal impedance of 10 MΩ, sensitivity of 0.1 mV). After the second injection, we let the Plexiglas column drained by gravity. The time-lapse self-potential measurements over the duration of the experiment are shown in Fig. 3.

Table 1
Summary of the result of the first self-potential experiment. This experiment comprises four increases and decreases of the imposed hydraulic head. The conductivity of the water is equal to 0.025 S m^{-1}. The experimental setup is shown in Fig. 2. The self-potential signal was recorded on a sand sample (20 cm long, $k = (9 \pm 2) \times 10^{-11}$ m^2, $\phi = 0.4$) with three silvers electrodes and a data-logger (Easy Log, internal impedance of 10 MΩ, sensitivity of 0.1 mV). The scanning electrodes were located at both ends of the sample while the reference was located in the mid-position inside the sample.

Water level (m)	Voltage (in mV)[a]	Voltage (in mV)[b]
0.5	−4.5	+7
1	−7.5	+7
1.8	−14	+11
1.7	−13	+10

[a] Located 10 cm above the reference (mV), upstream.
[b] Located 10 cm below the reference (mV), downstream.

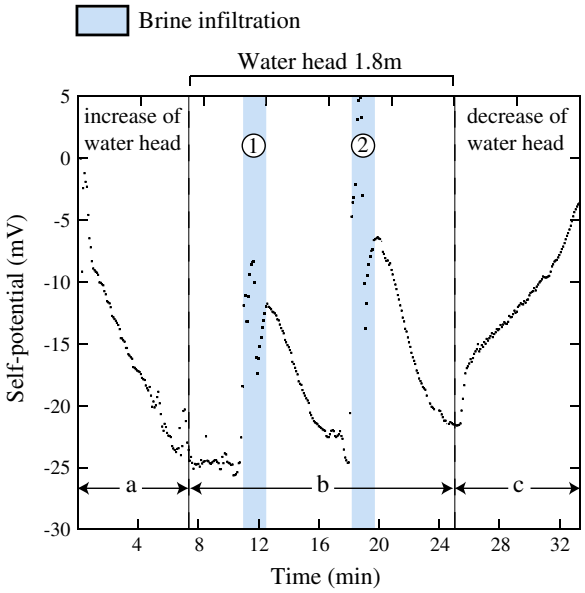

Fig. 3. Self-potential results of the brine injection experiment. This plot shows three distinct stages. (a) This stage concerns the increase of water head in the column. (b) This stage represents first the stabilisation phases for 1.80 m water pressure and then the injection of two brine solutions (blue stripes). (c) This stage shows the pipe draining.

We observe a transient decrease of the electrical potentials during the passage of the two brines. This result supports the theory that the injection of a high electrical conductivity solution σ_f decreases the electrical field. The change in the electrical response is instantaneous to the passage of the brine in the porous material.

We propose now a numerical simulation of the second brine injection using the commercial software COMSOL Multiphysics 3.3 (Comsol, 2007) which is a Partial Derivative Equation (PDE) solver based on the finite element method with triangular meshing. As described in Fig. 4, the forward modeling of a self-potential problem consists in the following steps (1) solving first the flow field, (2) solving the distribution of the salt concentration in the system by solving the advection–dispersion equation, (3)

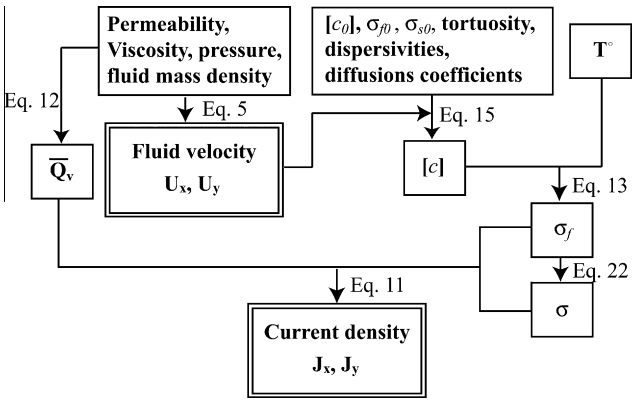

Fig. 4. Flowchart for the estimation of the current density field by numerical simulation. $[c_0]$ corresponds to the salt concentration of the brine solution, σ_{f0} and σ_{s0} corresponds respectively to the initial electrical conductivity of the water and the sand sample. The Fluid flow velocity field is determined using Darcy's equation (Eq. (5)) while the salt concentration is determined through the transport equation (Eq. (15)) using the fluid flow velocity field previously established. Eqs. (13) and (22) are used to estimate the water and sample electrical conductivity, respectively. The current density field distribution is finally determined using the excess of charge per unit pore volume with Eq. (11).

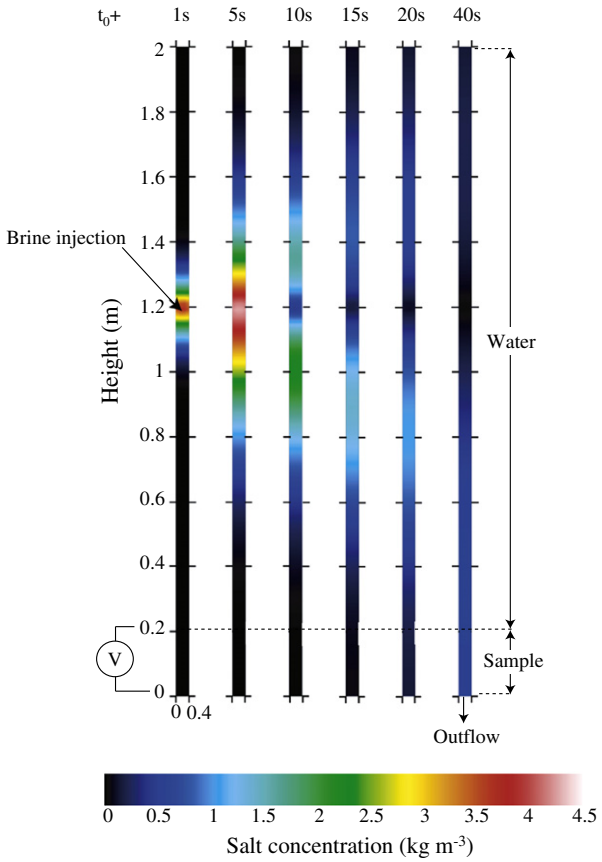

Fig. 5. 2D numerical modeling of the self-potential signal associated with the temporal evolution of the brine solution concentration inside the Plexiglas pipe (t_0: time of brine injection). This figure presents only the evolution of water salt concentration inside the column over the time. Variation of the simulated self-potential signal at end faces of the sample is shown in Fig. 6. The brine injection inside the column takes place at 1 m above the top of the sample. The color scale represents the salt concentration expressed in kg m^{-3}.

determining the volumetric source current density from the flow field information and (4) solving the Poisson equation for the electrical potential distribution using the volumetric source term and the change in conductivity associated with a change in salinity. During the simulation, the fluid mass density is assumed to be constant (and equal to 1000 kg m^{-3}). The influence of the density change is negligible here on the flow field because of the strong velocity associated with the hydrostatic pressure gradient and the short duration of the experiment.

The numerical simulation was performed in 2D in temporal condition with the finite element code COMSOL Multiphysics (Comsol, 2007) with approximately 2300 triangular elements. The model was composed of two subdomains which correspond to the water inside the column and the sand sample. The normal component of the Darcy velocity was specified to be null at the surface of the walls of the column (impervious boundary). A constant head boundary of 1.80 m was imposed above the sand sample and a null pressure (Dirichlet boundary condition) was imposed at the bottom of the column. For the transport problem, an isolation/symmetry boundary condition ($n \cdot N = 0$; $N = -D_m \nabla c + c\mathbf{u}$) was imposed at the surface of the wall of the column while adjective flux $n \cdot (\phi D_m \nabla c) = 0$ was imposed at the bottom of the column. For the electrical problem, insulating boundary conditions were applied at all boundaries.

Fig. 5 shows six numerical snapshots of the evolution of the salt solution concentration in the Plexiglas pipe over time (numerical resolution was performed between $t_0 = 0$ s and $t_f = 60$ s with a 1 s

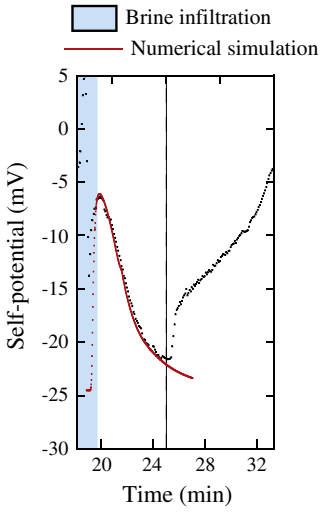

Fig. 6. Comparison between the self-potential data recorded during the second brine injection and the self-potential resulting from the numerical simulation. The simulated self-potential data was generated using an hydraulic permeability k equal to 7.25×10^{-11} m^2 and an excess of charge per unit pore volume $\overline{Q}_v$ equal to 0.13 C m^{-3} (measured permeability value and estimated excess of charge per unit pore volume for the sand are respectively $k = (9 \pm 2) \times 10^{-11}$ m^2 and $\overline{Q}_v = 0.11 \pm 0.02$ C m^{-3}). The self-potential data resulting from the numerical results match well with experimental self-potential data until 25 min. After 25 min the water pressure inside the column is no more maintain constant and the water pressure decreases progressively to reach a null pressure around 35 min. The modeling is performed for a constant hydraulic head inside the column and consequently does not take into account the water pressure decreases over time after $t = 25$ min.

time step). The brine injection takes place at a point in the center of the column (1 m above the sample) and the residence time of the salt in the column is approximately 10 s. Fig. 4 shows the increase of the size of the brine plume in the column and the decrease of the salt solution concentration over time. Fig. 6 shows a comparison between the numerical simulations (red line)[1] and the data. The concentration of the injected NaCl solution is 4.5 g L^{-1} (7×10^{-2} mol L^{-1}). This leads to a brine conductivity of 0.77 S m^{-1} using Eq. (12). Using different value of sample permeability k and according to the empirical powerlaw relationship between k and $\overline{Q}_v$ (Jardani et al., 2007; Bolève et al., 2009), a good fit was obtained by taking $k = 7.25 \times 10^{-11}$ m^2 (the measured permeability value for the sand is $k = (9 \pm 2) \times 10^{-11}$ m^2) and an excess of charge by unit pore volume $\overline{Q}_v \approx 0.13$ C m^{-3} (the estimated value using the measured coupling coefficient was $\overline{Q}_v = 0.11 \pm 0.02$ C m^{-3}, see above). In a laboratory sand column experiment, the longitudinal dispersivity α_1 is typically assumed to be in the range 1–10 cm (we used $\alpha_1 = 10$ cm), and the transversal dispersivity correspond to 1/5–1/100 α_1 (Bear, 1972) (this yields $\alpha_2 = 0.1$ cm).

This experience demonstrates the self-potential method can be used to monitor the flow of a salt tracer and can be used to determine the permeability along the flow path. In the next section, we apply this approach to a dam which presents a known leakage.

4. Field test

4.1. Field survey and results

The use of the self-potential monitoring of a salt tracer is now applied to a dam test site located in the south of France. This test site is composed by two basins separated by a dyke. The waterproof quality of the dam is ensured by concrete slabs (see Fig. 7). This dam records however losses of water with a flow rate of approximately 1 m^3 per second. The objectives of the field campaign were (1) to locate the leaking area using a self-potential mapping of the bottom of the basin and (2) to quantify the flow rate of leakage.

Fig. 6 shows a sketch of the dam and the self-potential map performed at the ground surface. For this test site, voltages were measured with a high impedance voltmeter (Metrix MX-20, internal impedance 100 MΩ, sensitivity of 0.1 mV) and Petiau Pb/$PbCl_2$ electrodes (Petiau, 2000). Visual inspection shows an important leakage at the south angle of the basin which due to the presence of cracks. At this location, the self-potential map shows a significant decrease of the electrical potential signal (from zero to about −55 mV). Such negative self-potential anomalies are a typical signature of leakages (see anomalies A1 and A2 in Fig. 7). Indeed, the contrast of the excess of charge per unit pore volume between the water in the basin ($\overline{Q}_v = 0$) and in the dam ($\overline{Q}_v \neq 0$) is responsible for a volumetric source current density explaining the polarity of the self-potential anomaly. The divergence of this current density produces a negative electrical field which can be measured at the floor of the basin.

We performed a brine injection using an array of non-polarizing electrodes to monitor the fluctuations of the self-potential signals at the crest of the dam. The network of electrodes covers entirely the south angle of the basin. These measurements were performed with two self-potential lines of non-polarizing electrodes. Each line consists of 16 non-polarizing Petiau electrodes (Petiau, 2000). The acquisitions were made with a National Instrument NI USB-6218 acquisition card (internal impedance of 10 GΩ). The measurements were recorded at a frequency of 200 Hz, averaged every second, and stored in a computer (Fig. 8).

The following experimental protocol was used. In a first stage, before brine injection, we considered that the flow was in steady-state conditions and we measured the self-potential signal at 200 Hz. We then performed two brine injections to monitor the response over time with the network of non-polarizing electrodes. Next, we subtracted the measured data from the reference self-potential data collected prior to the brine injection because we are only interested to the change over time of the self-potential response. In this case, the passage of the salt was expected to generate a positive self-potential anomaly with respect to the background value in time (Fig. 9). In parallel to these self-potential acquisitions, electrical conductivity of the seepage outflow was also monitored. The results of the electrical potential signal and water electrical conductivity monitoring are shown in Figs. 10 and 11, respectively.

During the monitoring, the self-potential signals exhibit two positive peaks corresponding to the passage of the two separated brine injections. These anomalies are located between electrodes #17 and #32, which are located on the road seawall which separates both basins. From the time difference between the brine injections and the occurrence of the peak of the self-potential anomaly (36 min), an estimate of the permeability k can be made using the distance between the brine injection and the self-potential electrodes (estimated to 10 m), a hydraulic head gradient of 0.6 between the two basins), we obtain $k = (10 \pm 5) \times 10^{-10}$ m^2. However, this estimate takes into account the time of brine injection in the basin and not the time of the brine infiltration in the leaking zone. Therefore it may underestimate the true permeability of the leaking area. Another determination of the permeability can be performed using the delay between the electrical self-potential anomaly and the peak of electrical conductivity of water resurgence (90 s). We find a permeability of approximately $(5 \pm 2) \times 10^{-8}$ m^2 (with a distance between brine injection and

[1] For interpretation of color in Figs. 3, 5–7, the reader is referred to the web version of this article.

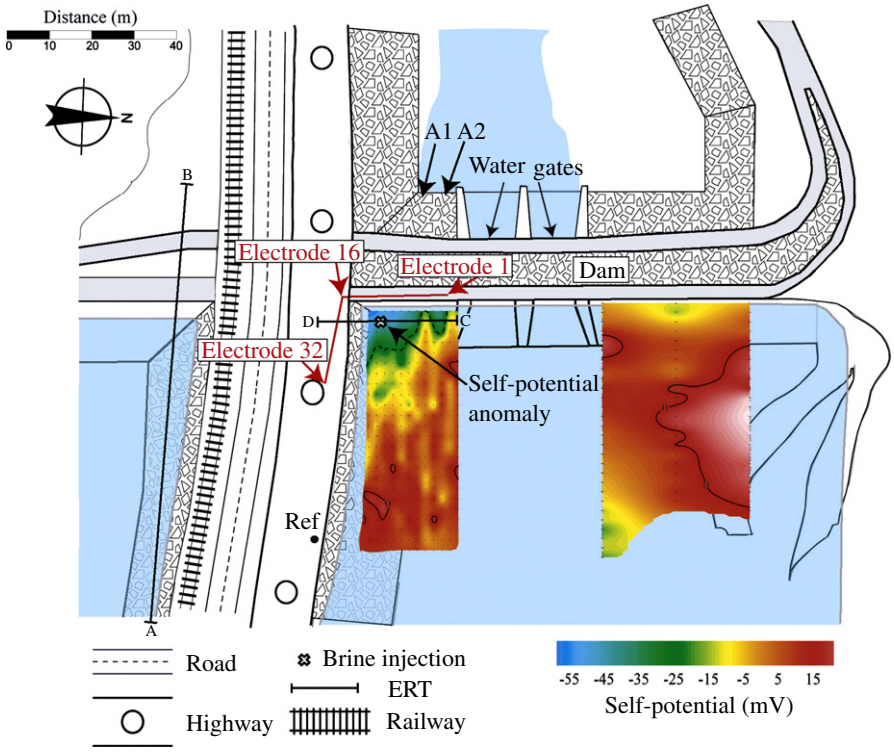

Fig. 7. Sketch of the test site, with self-potential maps superimposed and localization of the self-potential electrodes line (used for the monitoring) at the crest of the dam (red line). The self-potential data are recorded with a high impedance voltmeter (Metrix MX-20, internal impedance equal to 100 MΩ, sensitivity of 0.1 mV) and non-polarizable Petiau electrodes (Petiau, 2000). Labels A1 and A2 indicate the location of the leakage outflow that is observed by visual inspection. The position of the brine injection and the position of the two resistivity profiles are also indicated.

Fig. 8. Self-potential setting. The equipment consists of 2 cables of 16 non-polarizables Petiau electrodes connected to the acquisition system. The self-potential signals are recorded over time with a frequency f equal 200 Hz (signal averaged every second). The electrode spacing is equal to 2 m. In order to improve the electrical contact between the electrodes and the ground, water from the basins was used to decrease the contact resistance.

self-potential electrodes estimated to 25 m for a hydraulic gradient equal to 0.6), an estimate one order of magnitude larger than the previous one. This last estimate seems consistent with the flow rate lost from the decrease of the water level in the reservoir when all gates are closed.

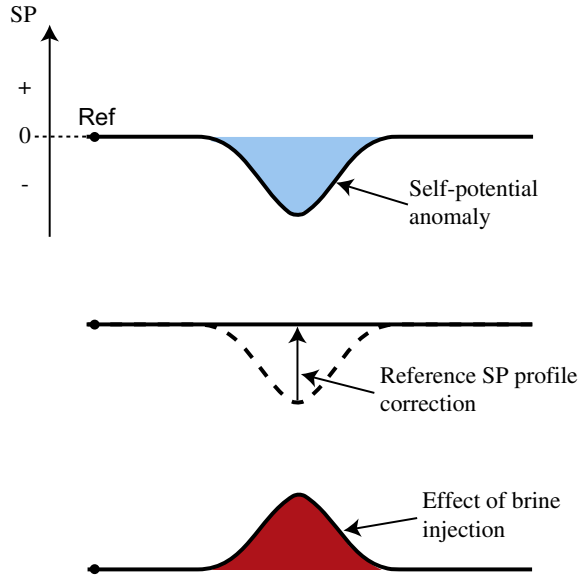

Fig. 9. Self-potential associated with the brine injection test. The negative self-potential anomaly is associated with the leakage inflow. All the self-potential signal is normalized by removing the initial self-potential data recorded before the brine injection. The brine injection is consequently view as a positive self-potential anomaly, which is only related to the leakage.

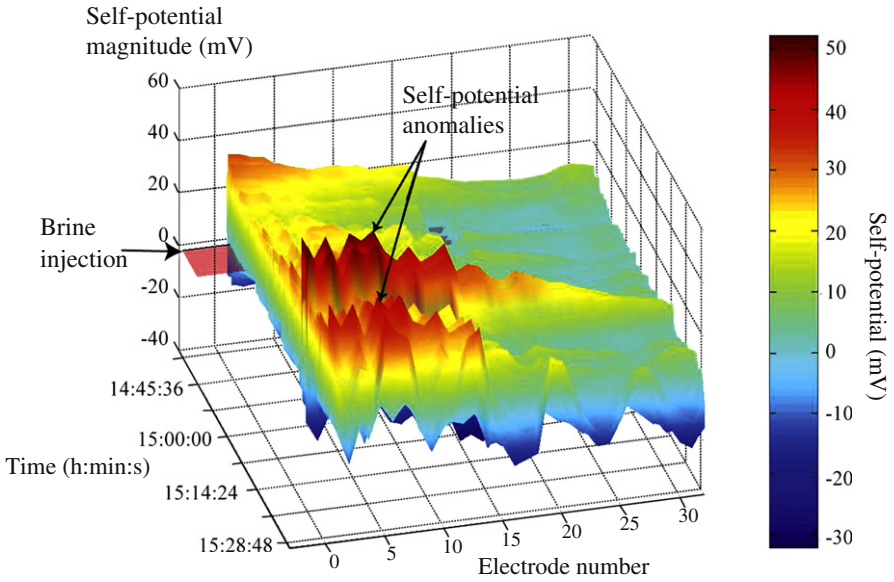

Fig. 10. Temporal variation of the normalized self-potential data at the crest of the dam. The two self-potential peaks can be related to the injection of the salt. The two positives peaks appear on electrodes #1–#16 (first cable). These positions coincide with the position of the negative self-potential anomaly shown by the self-potential map (inflow of the leakage) and the resurgence areas A1 and A2 (see Fig. 7). The permeability k of the flow path was estimated to 1×10^{-9} m^2 by taking into account the time-lapse between the brine injection and the first occurrence of the positive self-potential peak.

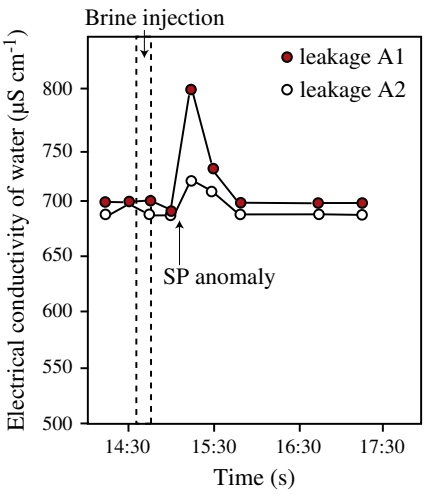

Fig. 11. Time variation of the electrical conductivity of the water at positions A1 and A2 (outflows). Note the good agreement between the order of the events including the salt injection, the occurrence of the self-potential anomaly, and finally the occurrence of the brine conductivity anomaly. By taking into account the time of occurrence of the self-potential positive anomaly and the time of the peak in the conductivity of the pore water electrical conductivity, we estimate the permeability k of this zone to be equal to 5×10^{-8} m^2.

4.2. Numerical simulations

In order to improve the estimation of the permeability of the leaking zone, a 3D numerical fluid flow simulation (in steady-state condition) was performed with Comsol Multiphysics 3.3. The numerical simulation consisted in solving first the Darcy's equation and then the electric problem within a realistic 3D geometry. In this simulation, we did not solve the transport equation because we are first interested to compare the computed self-potential map with the measured self-potential map (see Fig. 6) obtained prior the brine injection.

We include the resistivity distribution from the DC resistivity tomogram and used the self-potential map to constrain the numerical simulations. Our goal is to confirm the leakage area and its permeability. Regarding the geometry, the main and road dams are seated on alluvium beds as shown in Fig. 13. A seal was used in the numerical simulation to impose a no flow boundary condition in the absence of leakage. On the side of the embankment filled with water, the presence of mud located in between the alluviums and the water body was accounted for as shown by the interpretation of the DC resistivity tomography (Fig. 12). The leaking area is modeled as a simple pipe through the embankment at the corner between the road and the embankment (see Fig. 13). In this numerical simulation, we assume that the dam is made of a uniform material (concrete). Darcy's law was used to simulate the flow of the pore water (in saturated condition) inside the leakage area. Impermeable boundary conditions are imposed at all the boundaries (dam, seal, mud, and alluvium) except at the position of the leaking pipe where we imposed a hydraulic gradient i equal to 0.6. This value was determined according to field observations. Indeed, a constant head boundary of 5 m was imposed at the entrance of the leaking simulated pipe and a null pressure (Dirichlet boundary condition) was imposed at the exit. For the electrical problem, the value of the electrical resistivity is determined according to the DC resistivity tomography (see Fig. 12 and Table 2). For the computation of the self-potential data, a voltage reference (zero voltage) is setup at the same position where the field reference electrode is located. This is important to use the same voltage reference in order to be able to compare the numerical simulations of the self-potential field with the field measurements. The boundary condition at the contact with the atmosphere is an insulating boundary condition ($\hat{n} \cdot \mathbf{j} = 0$ where $\hat{n}$ is the outward normal vector at the water or sediment/atmosphere interface). The continuity boundary condition is imposed at all other boundaries of the system.

The numerical simulations are shown in Figs. 13 and 14. Fig. 13 shows the 3D distribution of the self-potential equi-potentials on the upstream side. We see clearly the self-potential anomaly resulting from the leakage zone. Fig. 14 shows a comparison between the two first rows of measured self-potential data along the road dam, and the self-potential data resulting from the numerical simulation. The permeability of this pipe was

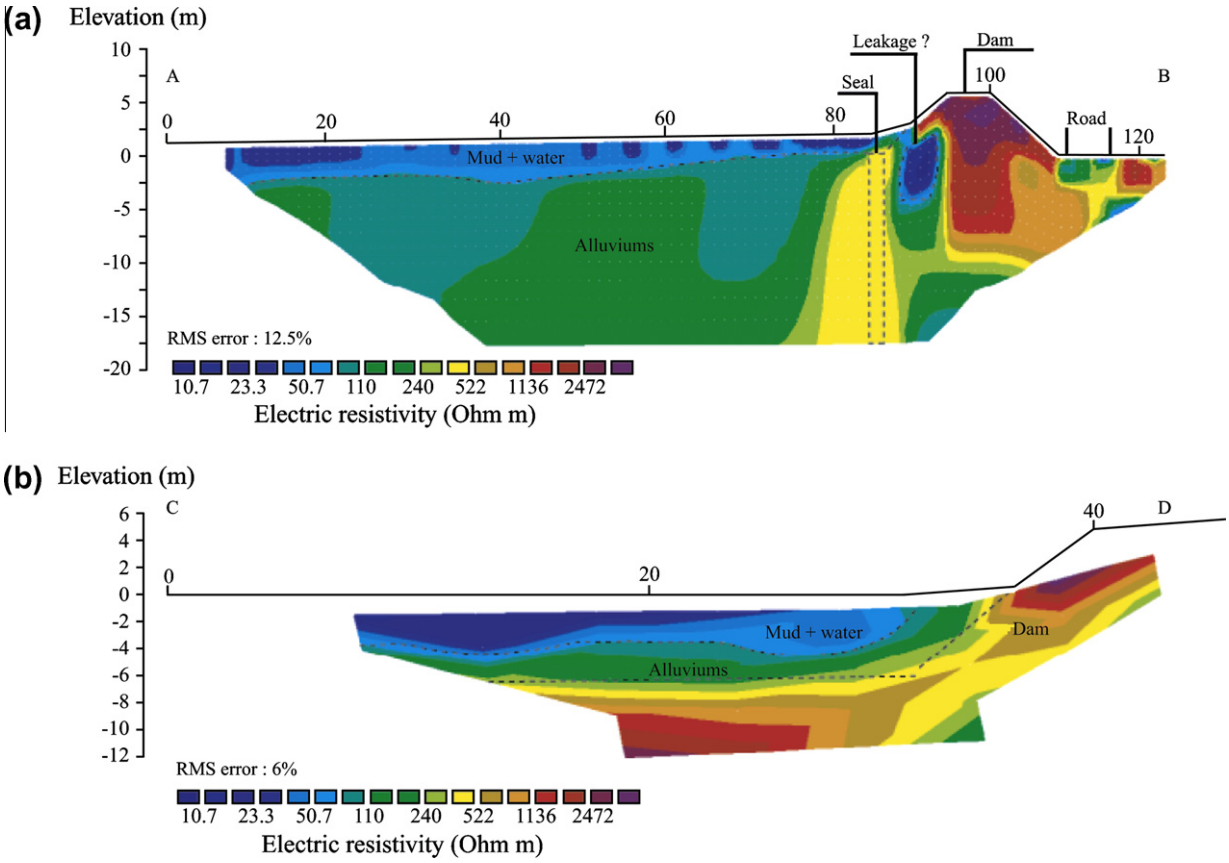

Fig. 12. Resistivity tomograms inverted using RES2DINV (Loke and Barker, 1996). We use a Wenner-α array and a take-out spacing of 5 m.

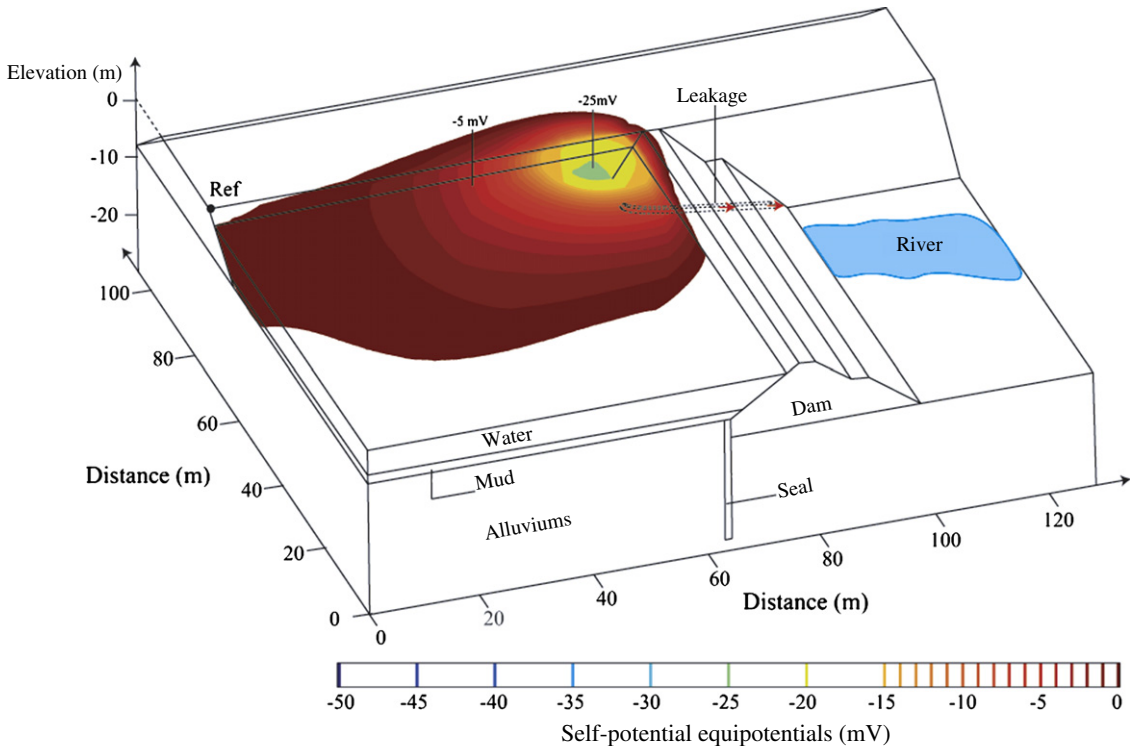

Fig. 13. 3D numerical simulation of the self-potential equipotential distribution associated with a leaking simulated cylindrical volume. The simulations are performed with COMSOL Multiphysics 3.3. The numerical simulation was performed in steady-state condition. The electrical resistivity values of the different domain (water, mud, alluviums, seal, and dam) are determinated using the two resistivity tomograms shown by Fig. 12 (see Table 2). The self-potential equipotentials result only from the ground water flow (without brine injection) along the cylindrical flow path with a permeability k equal to 5×10^{-8} m^2 (see Table 2).

Table 2
Electric resistivity values used for the 3D numerical simulation. For the fluid flow problem, the excess of charge per unit pore volume $\overline{Q}_v$ and the permeability k are evaluated only in the leakage zone where the streaming current is believed to be generated. For the electrical problem, the electrical conductivity is given for all domains in order to compute the equipotentials in 3D.

Parameters	Alluvium	Dam	Seal	Reservoir water	Mud	Leakage area
ρ (Ω m)	250	1500	500	50	50	150
Q_v (C m^{-3})	–	–	–	–	–	0.032
k (m^2)	–	–	–	–	–	5×10^{-8}

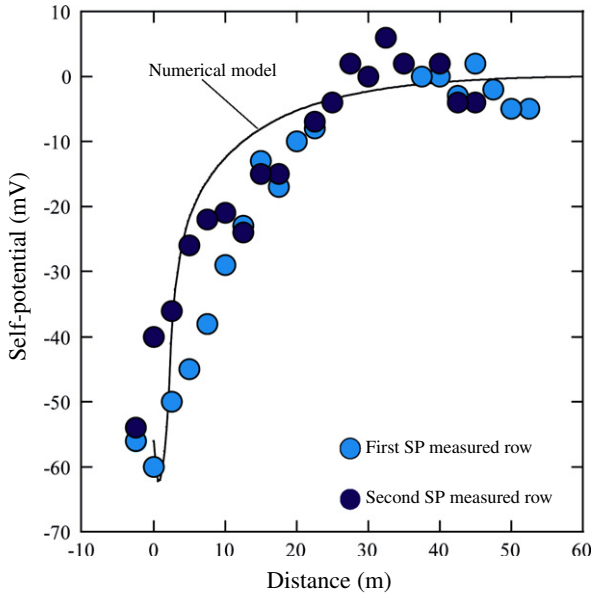

Fig. 14. Comparison between the modeled and the measured self-potential data. The measured values correspond to the two first rows of the south self-potential map shown in Fig. 6. The modeled data points are come from the 3D numerical simulation shown in Fig. 12. The leakage is associated with a −60 mV self-potential anomaly according to the reference electrode position. The good agreement with the observed and simulated results implies that the permeability estimate we used is correct.

progressively increased by trial and error until the resulting self-potential data matched the measured self-potentials (see Fig. 13). This trial and error test (modification of permeability value) yield a value for the permeability of the leaking area equal to 5×10^{-8} m^2 and an excess of charge per unit pore volume equal to 0.032 C m^{-3} (reported in Table 2). This permeability value agrees with the estimate established using the brine solution tracer ($k_1 = 5 \times 10^{-8}$ m^2) and is quite close to the estimate obtained from the time-lapse self-potential survey ($k_2 = 1 \times 10^{-9}$ m^2). However, this estimate of permeability is consistent with a high value of the excess of charge per unit pore volume. This can be explained only if clay materials inside the leaking area are present. This clay fraction may come from the mud layer revealed by the electrical resistivity tomography (Figs. 9 and 10). Using a hydraulic gradient i equal to 0.6 and a hydraulic permeability k equal to 5×10^{-8} m^2, the seepage velocity in the leakage area is estimated at 0.3 m s^{-1}. This agrees with the seepage velocity estimate (in the range of several centimeters per second) previously obtained using the brine solution injection test.

5. Conclusions

For the first time, the self-potential method associated with a brine injection has been successfully used to locate a leak in a dam and to estimate the permeability of the preferential fluid flow pathway. The advantage of this self-potential approach is that it is real time (this is not the case of DC resistivity monitoring) and can be therefore used to estimate the permeability of leakages characterized by high flow rates. Moreover, the easiness of implementation of the method, the simplicity and low-cost of the equipment as well as the interpretation procedure, makes this approach a promising method to monitor dams and embankments and to estimate permeability along the flow paths. The next step will be to develop a time-lapse hydraulic tomography using the self-potential data as input data and background electrical resistivity tomography.

Acknowledgments

This work was supported by ANR Project ERINOH in France related to the study of leakage in embankments dams. The Ph-D Thesis of A. Bolève was supported by ANR and FUGRO through a Ph-D fellowship. We thank EDF for access to their site and their financial and scientific support. We thank Jean Vandemeulebrouck, Damien Jougnot (Université de Savoie) and Scott Ikard (Colorado School of Mines) for fruitful discussions. We thank NSF for funding the SmartGeo Educational Program (Project IGERT: Intelligent Geosystems; DGE-0801692). A. Bolève thanks David Marsan (Université de Savoie) for his support.

References

AlSaigh, N.H., Mohammed, Z.S., Dahham, M.S., 1994. Detection of water leakage from dams by self-potential method. Eng. Geol. 37 (2), 115–121.
Bear, J., 1972. Dynamics of Fluids in Porous Media. Elsevier Scientific Publishing Co.
Bogoslovsky, V.A., Ogilvy, V.A., 1970. Natural potential anomalies as a quantitative index of the role of water seepage from reservoir. Geophys. Prospect. 18, 261–268.
Bolève, A., Revil, A., Janod, F., Mattiuzzo, J.L., Jardani, A., 2007. Forward modelling and validation of a new formulation to compute self-potential signals associated with ground water flow. Hydrol. Earth Syst. Sci. 11 (5), 1661–1671.
Bolève, A., Revil, A., Janod, F., Mattiuzzo, J.L., Fry, J.-J., 2009. Preferential fluid flow pathways in embankment dams imaged by self-potential tomography. Near Surf. Geophys. 7, 447–462.
Comsol, 2007. <http://www.comsol.com/>.
Corwin, R.F., 1985. The self-potential method and its engineering applications – an overview. Geophysics 50 (2), 282.
Corwin, R.F., 1997. The self-potential method for environmental and engineering applications: geotechnical and environmental geophysics. In: Ward, H. (Ed.), Investigations in Geophysics, Soc. Expl. Geophys., vol. 5, p. 1.
Crespy, A., Bolève, A., Revil, A., 2007. Influence of the Dukhin and Reynolds numbers on the apparent zeta potential of granular media. J. Colloid Interf. Sci. 305, 188–194.
Fell, R., MacGregor, P., Stapledon, D., 1992. Geotechnical Engineering of Embankment Dams. Balkema, Rotterdam, 675 pp. ISBN 90 5410 128 8.
Gex, P., 1980. Electrofiltration phenomena associated with several dam sites. Bull. Soc. Vaud Sci. Nat. 357 (75), 39–50.
Helmholz, H., 1879. Study concerning electrical boundary layers. Weidemann Ann. Phys. Chem. 3rd Ser. 7, 337–382.
Ishido, T., Mizutani, H., 1981. Experimental and theoretical basis of electrokinetic phenomena in rock–water systems and its application to geophysics. J. Geophys. Res. 86, 1763–1775.
Jardani, A., Revil, A., 2009. Stochastic joint inversion of temperature and self-potential data. Geophys. J. Int. 179 (1), 640–654.
Jardani, A., Revil, A., Bolève, A., Dupont, J.P., Barrash, W., Malama, B., 2007. Tomography of groundwater flow from self-potential (SP) data. Geophys. Res. Lett. 34.
Kosmulski, M., Dahlsten, P., 2006. High ionic strength electrokinetics of clay minerals. Colloids Surf. A: Physicochem. Eng. Aspects 291, 212–218.
Leroy, P., Revil, A., 2004. A triple layer model of the surface electrochemical properties of clay minerals. J. Colloid Interf. Sci. 270 (2), 371–380.
Leroy, P., Revil, A., 2009. Spectral induced polarization of clays and clay-rocks. J. Geophys. Res. 114, B10202.
Loke, M.H., Barker, R.D., 1996. Rapid least-squares inversion of apparent resistivity pseudosections by quasi-Newton method. Geophys. Prospect. 44, 131–152.
Martínez-Pagán, P., Jardani, A., Revil, A., Haas, A., 2010. Self-potential monitoring of a salt plume. Geophysics 75 (4), WA17–WA25.
Mitchell, J.K., 1993. Fundamentals of Soil Behavior. John Wiley & Sons, New York, p. 437.
Morgan, F.D., Williams, E.R., Madden, T.R., 1989. Streaming potential properties of westerly granite with applications. J. Geophys. Res. 94, 12449–12461.

Müller, K., Vanderborght, J., Englert, A., Kemna, A., Huisman, J.A., Rings, J., Vereecken, H., 2010. Imaging and characterization of solute transport during two tracer tests in a shallow aquifer using electrical resistivity tomography and multilevel groundwater samplers. Water Resour. Res. 46.

Nourbehecht, B., 1963. Irreversible thermodynamic effects in inhomogeneous media and their applications in certain geoelectric problems. Ph.D. Thesis, Mass. Inst. of Technol., Cambridge, Mass.

Panthulu, T.V., Krishnaiah, C., Shirke, J.M., 2001. Detection of seepage paths in earth dams using self-potential and electrical resistivity methods. Eng. Geol. 59 (3–4), 281–295.

Petiau, G., 2000. Second generation of lead–lead chloride electrodes for geophysical applications. Pure Appl. Geophys. 157, 357–382.

Rath, V., Mottaghy, D., 2007. Smooth inversion for ground surface temperature histories: estimating the optimum regularization parameter by generalized cross-validation. Geophys. J. Int. 171 (3), 1440–1448.

Revil, A., 2007. Thermodynamics of transport of ions and water in charged and deformable porous media. J. Colloid Interf. Sci. 307 (1), 254–264.

Revil, A., Jardani, A., 2010. Stochastic inversion of permeability and dispersivities from time lapse self-potential measurements: a controlled sandbox study. Geophys. Res. Lett. 37, L11404.

Revil, A., Leroy, P., 2004. Governing equations for ionic transport in porous shales. J. Geophys. Res. 109, B03208.

Revil, A., Linde, N., 2006. Chemico-electromechanical coupling in microporous media. J. Colloid Interf. Sci. 302, 682–694.

Revil, A., Cathles, L.M., Losh, S., Nunn, J.A., 1998. Electrical conductivity in shaly sands with geophysical applications. J. Geophys. Res. 103 (B10), 23925–23936.

Revil, A., Pezard, P.A., Glover, P.W.J., 1999a. Streaming potential in porous media. 1. Theory of the zeta-potential. J. Geophys. Res. 104 (B9), 20021–20031.

Revil, A., Schwaeger, H., Cathles, L.M., Manhardt, P., 1999b. Streaming potential in porous media. 2. Theory and application to geothermal systems. J. Geophys. Res. 104 (B9), 20033–20048.

Rozycki, A., 2009. Evaluation of the streaming potential effect of piping phenomena using a finite cylinder model. Eng. Geol. 104 (1–2), 98–108.

Rozycki, A., Fonticiella, J.M.R., Cuadra, A., 2006. Detection and evaluation of horizontal fractures in Earth dams using self-potential method. Eng. Geol. 82 (3), 145–153.

Sen, P.N., Goode, P.A., 1992. Influence of temperature on electrical conductivity of shaly sands. Geophys. 57, 89–96.

Sheffer, M.R., 2002. Response of the self-potential method to changing seepage conditions in embankments dams. M.A.Sc. Thesis, Dept. of Civil Eng., University of British Columbia.

Sheffer, M., 2007. Forward modeling and inversion of streaming potential for the interpretation of hydraulic conditions from self-potential data. Ph.D. Thesis, the University of British Columbia.

Sill, W.R., 1983. Self-potential modeling from primary flows. Geophysics 48 (1), 76–86.

Sjodahl, P., Dahlin, T., Johansson, S., 2005. Using resistivity measurements for dam safety evaluation at Enemossen tailings dam in southern Sweden. Environ. Geol. 49 (2), 267–273.

Sjodahl, P., Dahlin, T., Zhou, B., 2006. 2.5D resistivity modeling of embankment dams to assess influence from geometry and material properties. Geophysics 71 (3), G107–G114.

Titov, K., Loukhmanov, V., Potapov, A., 2000. Monitoring of water seepage from a reservoir using resistivity and self-polarization methods: case history of the Petergoph fountain water supply system. First Break 18, 431–435.

Wan, C.F., Fell, R., 2008. Assessing the potential of internal instability and suffusion in embankment dams and their foundations. J. Geotech. Geoenviron. Eng. 134 (3), 401–407.

Wilt, M.J., Corwin, R.F., 1989. Numerical modeling of self-potential anomalies due to leaky dams: model and field examples. In: Merkler, G.P. et al. (Eds.), Lecture Notes in Earth Science, Detection of Subsurface Flow Phenomena, vol. 27. Springer-Verlag, Berlin, Heidelberg, pp. 73–89.

Wurmstich, B., Morgan, F.D., Merkler, G.-P., Lytton, R., 1991. Finite-element modelling of streaming potential due to seepage: study of a dam. Soc. Explor., Geophysicists Technical Program Expanded Abstracts 10, 542–544.